



This is a repository copy of *Mechanical properties of stochastically cracked soft magnetic material*.

White Rose Research Online URL for this paper:

<https://eprints.whiterose.ac.uk/209204/>

Version: Published Version

---

**Article:**

Goodall, A.D. [orcid.org/0000-0002-4773-0321](https://orcid.org/0000-0002-4773-0321), Uramowski, J., Sinclair, C.W. et al. (2 more authors) (2023) Mechanical properties of stochastically cracked soft magnetic material. Additive Manufacturing Letters, 7. 100179. ISSN 2772-3690

<https://doi.org/10.1016/j.addlet.2023.100179>

---

**Reuse**

This article is distributed under the terms of the Creative Commons Attribution (CC BY) licence. This licence allows you to distribute, remix, tweak, and build upon the work, even commercially, as long as you credit the authors for the original work. More information and the full terms of the licence here:

<https://creativecommons.org/licenses/>

**Takedown**

If you consider content in White Rose Research Online to be in breach of UK law, please notify us by emailing [eprints@whiterose.ac.uk](mailto:eprints@whiterose.ac.uk) including the URL of the record and the reason for the withdrawal request.



[eprints@whiterose.ac.uk](mailto:eprints@whiterose.ac.uk)  
<https://eprints.whiterose.ac.uk/>



## Short Communication

## Mechanical properties of stochastically cracked soft magnetic material

Alexander D. Goodall<sup>a,\*</sup>, Jared Uramowski<sup>b</sup>, Chad W Sinclair<sup>b</sup>, Lova Chechik<sup>a</sup>, Iain Todd<sup>a</sup><sup>a</sup> Department of Materials Science and Engineering, University of Sheffield, Sheffield, UK<sup>b</sup> Department of Materials Engineering, The University of British Columbia, Vancouver, Canada

## ARTICLE INFO

## Keywords:

Laser powder bed fusion  
Cracking  
Soft-Magnetic material  
Mechanical characterisation  
FeSi

## ABSTRACT

Processing of soft magnetic materials with additive manufacturing has shown capability to deliver good magnetic properties and increased silicon content of Fe-6.5 wt%Si, however methods must be used to reduce the eddy currents in large bulk cross-sections in components created by additive manufacturing. Geometrical design has been shown to do this effectively, however stochastically cracked parts show similar magnetic performance with a large increase in stacking factor. To enable their use in electrical machines the mechanical properties of this material must be understood. Therefore, this study uses uniaxial tensile testing to understand the mechanical performance. The ultimate tensile strength of the material in the as-built condition was 17.9 MPa ( $\sigma = 4.5$  MPa), which was improved by 40% to 25.5 MPa ( $\sigma = 5.7$  MPa) by infiltrating the cracks with a low viscosity resin. This brings the material strength to more than three standard deviations from the required strength of 7 MPa to be used in a specific axial flux machine. The material exhibited an elongation to failure of 8-10%, showing that the suppression of ordered phases by high cooling rates has improved the ductility of the material. Hence, the stochastically cracked parts have sufficient properties to be used in the 3D magnetic circuits of electrical machines.

## 1. Introduction

Additive manufacturing (AM) has recently been used to process soft-magnetic materials such as FeSi [1], FeNi [2] and FeCo [3], showing sufficient magnetic properties [4,5] for usefulness in electrical machines (EMs). Mechanical properties such as elastic modulus, ultimate tensile strength (UTS) and elongation are rarely reported for these alloys after processing by AM. FeSi is the most common soft-magnetic material and normally has low silicon content around 3 wt%, where the alloy avoids brittle ordered phases B2 and D03 [6] during processing, allowing the alloy to be rolled into thin sheets. At 3 wt% silicon content the elongation is 8-11%, and UTS is 310-357 MPa [7]. Higher silicon content such as 6.5 wt% has been shown to improve certain magnetic properties such as higher resistivity and lower magnetostriction, and as such is promising for future use in efficient EMs [8]. Higher silicon content, however, means that brittle ordered phases will form during normal cooling [8], creating difficulties in processing the material into the thin sheets that are commonly used in EMs. Other methods have been used to enable processing of 6.5 wt%Si content such as post-rolling diffusion of silicon into Fe-3 wt%Si [9], however there is yet to be any scalable technology that allows processing of homogenous Fe-6.5 wt%Si. At

6.5% silicon content the elongation to failure and strength is decreased [10]. AM has a very high cooling rate, enabling some alloys such as binary FeCo to exhibit improved ductility by suppressing the brittle ordered phases formed under normal cooling conditions [11]. Currently, no such study has been completed on FeSi, but it is possible that a similar effect could be found.

To enable their use in alternating current (AC) EMs, soft-magnetic material is normally rolled into thin sheets to reduce parasitic eddy current losses. Similarly with AM, processing large bulk sections should be avoided, and therefore some cross-sectional geometries have been explored which achieve this such as lamination style slots [4], Hilbert space filling curve based cross-sections [5,12-14], and others [15-17]. In a recent work [18], the current author has shown that good magnetic performance can be achieved by utilising processing parameters to induce stochastic cracking of Fe-6.5 wt%Si, reducing eddy current losses and demonstrating improved performance when compared to designed geometries such as Hilbert space filling. To enable the adoption of this technology and use in an EM, the mechanical properties of this material must be understood.

In an EM, the stator or soft-magnetic core has relatively low mechanical requirements. This part is usually not rotating or structurally

\* Corresponding author.

E-mail address: [adgoodall1@sheffield.ac.uk](mailto:adgoodall1@sheffield.ac.uk) (A.D. Goodall).<https://doi.org/10.1016/j.addlet.2023.100179>

Received 14 July 2023; Received in revised form 7 September 2023; Accepted 12 October 2023

Available online 13 October 2023

2772-3690/Crown Copyright © 2023 Published by Elsevier B.V. This is an open access article under the CC BY license (<http://creativecommons.org/licenses/by/4.0/>).

stressed, therefore the only loading on the component is the forces from the magnetic circuit. Axial flux motors are a natural application for soft magnetic material processed by AM, as the 3D flux pathways increase the difficulties of using thin laminations making AM more appealing. In a motor designed by Nishanth et al [19], the tensile load requirements are 900 N for a cross-sectional area of 130 mm<sup>2</sup>, hence the stator tooth must survive a maximum stress of approximately 7 MPa.

In this study, the mechanical response in uniaxial tension of the stochastically cracked material is investigated, to determine if the strength of the material is sufficient for use in the stator of an electrical machine. Digital image correlation (DIC) is used to estimate the local strain values and inspect the failure modes of the material in uniaxial tension, as the material is highly non-uniform with a number of stress concentrations. The variability is assessed, and a method to improve the materials robustness and mechanical properties is proposed, wherein the cracks are filled with epoxy resin.

## 2. Materials and methods

### 2.1. Sample manufacture

Samples used in this study were created using Fe-6.5 wt%Si powder supplied by Höganäs, with a particle size of 15-45 µm. This powder was processed on an AconityMINI (Aconity3D GmbH) laser powder-bed fusion machine, equipped with a 200 W ytterbium doped continuous wavelength laser (wavelength 1074 nm) with a spot size of 70 µm. Samples were manufactured directly onto stainless steel build platforms, followed by sample removal using wire electrical discharge machining (EDM). Laser power of 195 W and laser speed of 0.4 m/s was used for stochastically cracked regions, whereas laser power of 140 W and laser speed of 0.7 m/s was used for solid regions of high density. Both regions use a layer thickness of 30 µm and a hatch spacing of 100 µm. The scan strategy used was 5mm wide stripes, with a layer rotation of 90° for stochastic cracked regions which refers to the parameter set 8\_400\_SR detailed in the authors recent study [18], and 67° for solid regions.

Tensile test samples were built by creating a 25 × 25 × 10 mm stochastically cracked region, flanked by 25 × 25 × 10 mm solid regions as per Fig. 1. These sections were interlocked with a 2 mm wide region which alternated between solid and cracked every second layer. This provided a structurally sound joint between regions, allowing the sample to fracture within the gauge length rather than at the weld line between the regions. Flat tensile test samples were then machined from these blocks via EDM, cutting the tensile test bar outline first, with a gauge length of 10 mm, gauge width of 6 mm and a corner radius of 6.5 mm, then slicing into samples 3 mm thick, giving approximately 18 mm<sup>2</sup> cross-sectional area in the gauge length. This was measured for each sample with a set of digital callipers.

Solid tensile test samples were also built using the parameters for the solid region throughout the whole part. These were then machined into

the same sample size using EDM.

### 2.2. Tensile test and DIC

Tensile testing was performed on an Instron 8896 Universal Testing Machine, with a 25 kN load cell. Samples were deformed at a constant rate of 0.005 mm/s until fracture, while the load and crosshead extension were recorded at a rate of 10 Hz. Samples were pre-loaded to no more than 100 N prior to testing, thereby eliminating any fixture slip and ensuring the sample was adequately seated in the grips.

Due to the highly non-uniform distribution of cracks in the material, strain was measured using both gauge length extension and optical DIC. A pattern was created using aerosol paint, first applying a white background before carefully applying the black speckle pattern. A consistent pattern was created for all samples, giving acceptable spatial resolution for displacement field calculation. On average, the size of each speckle was 0.35 mm and spaced by 0.3 mm. The system was calibrated for displacement and corrected for the camera angle using a standard 2.5 mm spaced grid pattern of 1 mm crosses. Images were taken with a LaVision Imager QE camera through a 60 mm lens at an aperture of 5.6, acquired at a rate of 5 Hz for the duration of the test, storing the load data for each image. The distribution of strain was visualized using DaVis version 10 software, where images were processed using the sum of differential method, at a subset and step size of 23 and 7 pixels respectively.

Due to noise in the data, smoothing was applied to the results to allow for better clarity. A Lowess method was applied using a span of 10 data points. For solid samples this was applied over the whole range. For the stochastic cracked samples, the data was split into 3 sections to avoid reducing the value of the UTS due to smoothing. The three sections were the region until the first failure, the plateau between the first and second failures and the section after the second failure. The impact of this smoothing can be observed in Fig. 3b. Strain was obtained by using cross head extension/gauge length.

### 2.3. Epoxy resin reinforcement

Filling of the cracks with epoxy resin was attempted to improve the mechanical performance of the stochastically cracked samples. An ultra-low viscosity epoxy was used from NextStar [20] to allow the epoxy to penetrate the microscopic cracks. The epoxy was applied by submerging the samples in a vat of resin, then placing inside a vacuum chamber for 30 minutes. Following this the epoxy was allowed to cure for approximately 5 hours at room temperature, at which point the viscosity of the epoxy had increased significantly. The samples were then removed from the vat of epoxy, whereby the excess epoxy could drain from the exterior surfaces of the sample, with the assumption that any epoxy inside the cracks would have too high of a viscosity to leave the sample. The samples reinforced with epoxy were then left to cure for the remainder of the four-day cure time.

## 3. Results

### 3.1. Tensile test results, solid

Tensile testing was conducted on 5 samples which were built using parameters intended for solid material without any cracks. These were tested to give a baseline to compare the stochastically cracked samples to, as there are no studies in literature characterising Fe-6.5 wt%Si, manufactured by AM. Stress-strain data is shown in Fig. 2. The average UTS was 56.7 MPa with a standard deviation of 6.4 MPa. The average elastic modulus was 98.2 GPa, with a standard deviation of 6.7 GPa, found using a linear fit on the data below 30 MPa to stay in the linear region, as the 0.2% strain measurement is unsuitable for this material. Sample B was excluded from the elastic modulus calculation due to the high stress at the start of the test of 31.0 MPa. Data has been

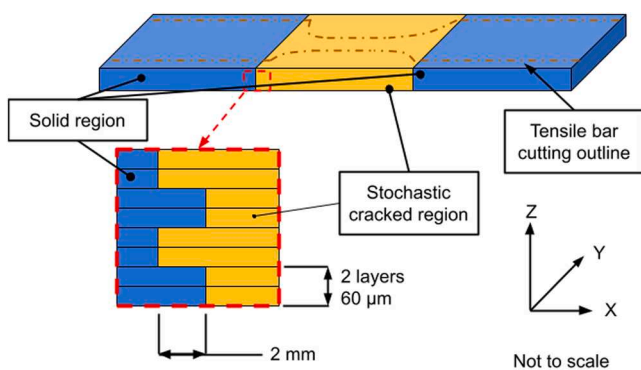
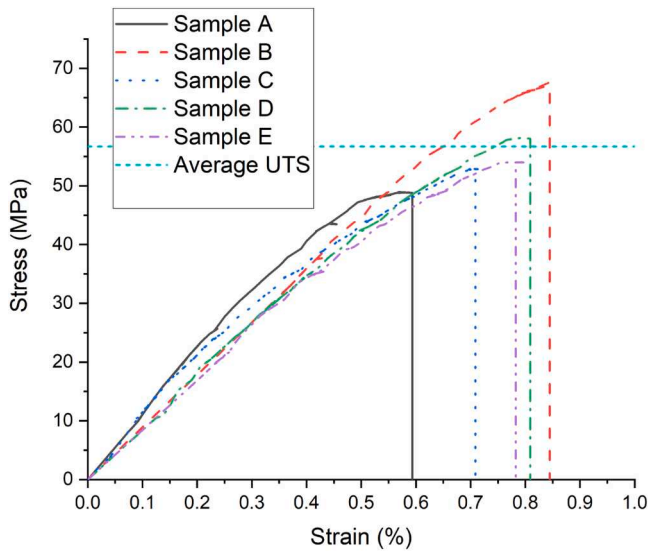


Fig. 1. Details of the additively manufactured blocks, from which tensile test samples were machined.



**Fig. 2.** Tensile test results of as-built Fe-6.5 wt%Si with solid cross-section, showing an average UTS of 56.7 MPa.

extrapolated to start at the origin of the stress strain graph as shown in Fig. 2.

### 3.2. Tensile test results, stochastically cracked

Tensile testing was conducted on 8 samples with stochastic cracking

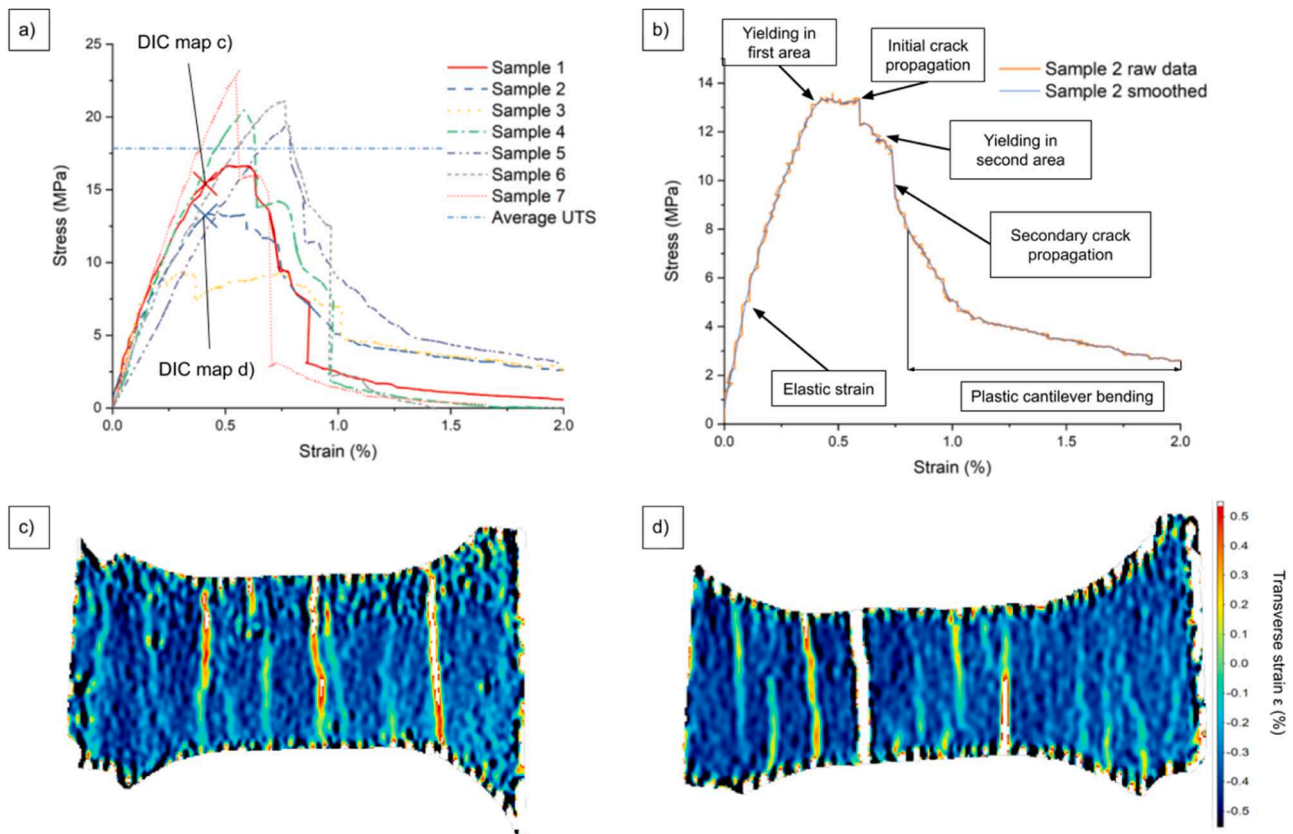


**Fig. 3.** Tensile test results showing stress vs strain (a). All samples show a linear elastic region, followed by a small area of yielding and a sharp decrease in stress carrying capacity. The effect of data smoothing is shown in (b) along with the suspected failure modes of each area of the curve. Stress concentrates into distinct bands, with examples from sample 1 as shown(c) and sample 2 (d), demonstrating the likelihood of underlying cracks perpendicular to the force. Areas of white have exceeded the scale and are not yet cracks.

in the as-built condition. One of the samples has been excluded from the results as it fractured outside of the gauge length along the radius between the gauge length and clamping face. The remaining samples show an unusual stress-strain curve (Fig. 3a) starting with a linear elastic region, with a small area of yield followed by failure at ultimate tensile stress (UTS). After this failure the stress-strain curve continues with at least one lower plateau, followed by a gradual decrease to zero-stress. The samples show an average UTS of 17.9 MPa, with a standard deviation of 4.5 MPa. The minimum recorded UTS was 9.6 MPa for sample 7. Strain in the samples is concentrated into distinct bands, perpendicular to the loading direction due to the pre-existing cracks in the material causing distinct changes in cross-sectional area (Fig. 3c/d).

DIC was used to show the strain behaviour throughout the test. By using the raw images to observe the cracks in the gauge section, and the processed images to find the strain, a deeper understanding of the stress curve in Fig. 3b is obtained. There is a region of linear elastic strain initially. An effective elastic modulus can be calculated from this linear region; however, the strain is highly non-uniform (Fig. 4a-c) and the effective cross-sectional area is unknown, therefore this is a property of the system rather than a material property. The average elastic modulus is 4.9 GPa with a standard deviation of 1.4 GPa. Following the linear elastic region there is a small region of plastic deformation where the material yields. Yield stress is normally quoted as a proof stress, an offset of the linear elastic region starting at a strain of 0.2%. This is an unsuitable measure for these samples as this would often be beyond the UTS. The next significant area on the curve is the first failure or crack initiation which can be observed in the DIC images (Fig. 4d-f). XCT shows that there are pre-existing cracks in the material [18], therefore these images show the point at which this crack propagates to the external surface and hence the material can no longer take load in this

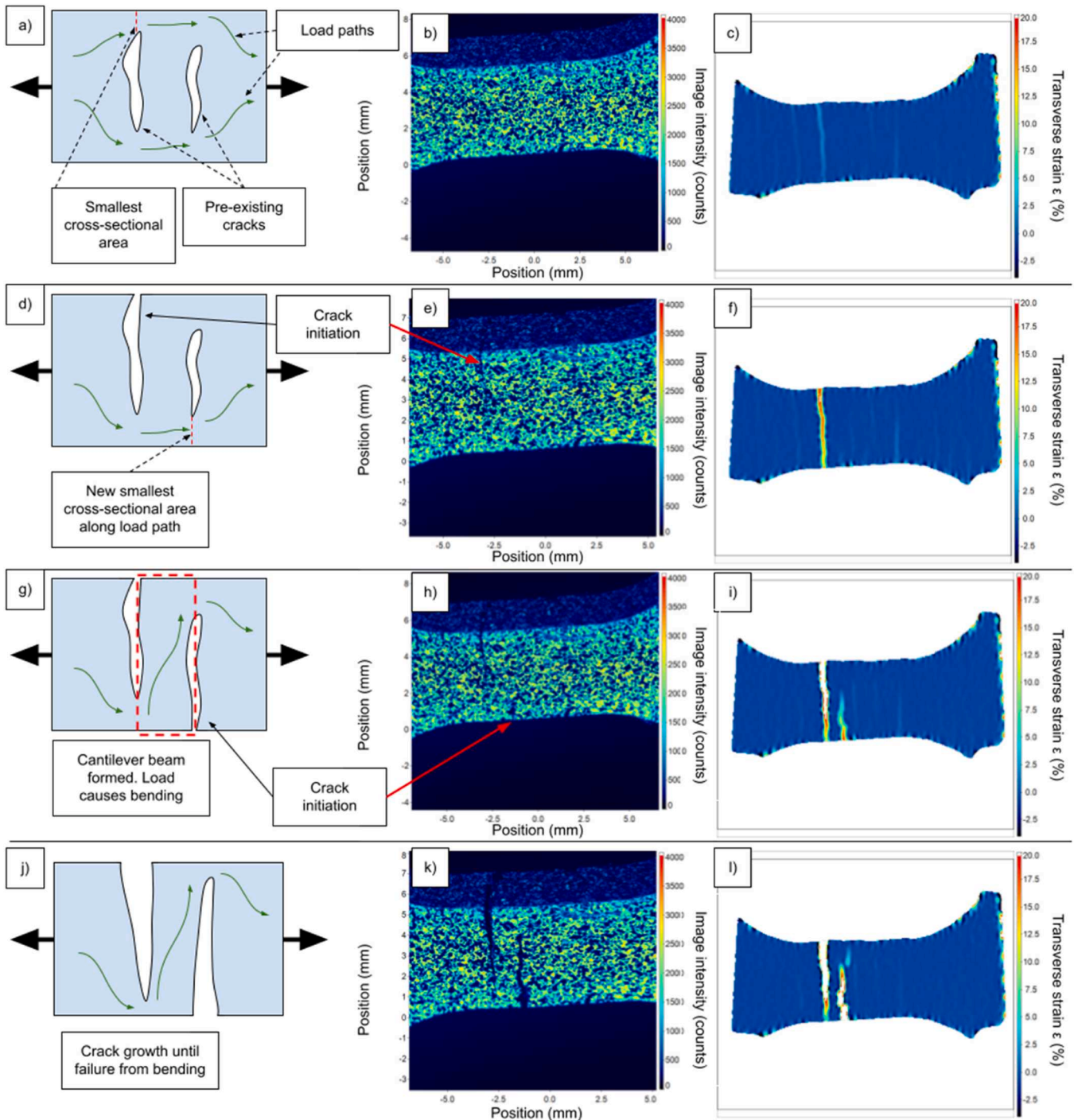


Fig. 4. DIC showing the progression of cracks through the gauge section of sample 2, along with simplified sketches explaining the strain patterns observed. The middle column is the raw DIC image, and the right hand column is the process strain data of the same frames.

area. This appears to happen with very little yield; however, it is not possible to conclude that the material is demonstrating a brittle failure due to noisy data. As the average elastic modulus is at least an order of magnitude smaller than the expected value for non-ordered Fe-6.5 wt% Si of 100 GPa, found in both literature [21] and by tests on solid components, we can conclude that the stress is concentrated into a much smaller cross-sectional area than the full gauge section.

Once this first crack has penetrated to the surface, there appears to still be load carrying capacity which must occur on the other side of the pre-existing crack. At this point, it is hypothesised that there is movement in both the first crack continuing to propagate, and a second area

of material yielding. Following this there is another distinct failure where the stress carrying capacity drops instantly, which is believed to be a second crack opening (Fig. 4g-i). It is likely that this will happen on the opposite side of the gauge section than the first crack, as the first crack will stop the load path along this edge. Following this second crack, a cantilever beam type scenario occurs, whereby there is a beam which is fixed at both ends with a perpendicular force at each end (Fig. 4j-l). This has significantly less resistance to axial stress and hence a lower stress carrying capacity, however it allows large displacements before one of the cracks eventually propagates all the way through the cross-section when the stress drops to zero. The raw DIC capture

showing the crack propagation can be found in [Video 1](#).

During additive manufacturing, the high cooling rates have been shown to suppress the ordered phases B2 and D03 in Fe-6.5 wt%Si [1]. These ordered phases are responsible for the brittle behaviour of this alloy, therefore if these phases are suppressed it is possible that the ductility of the material will increase. From DIC data it is possible to observe the local strain before crack propagation which is recorded at 8-10%, as shown in [Fig. 5](#) for sample 6 but is similar for all the samples. This finding requires further validation from bulk samples without cracks, and using a finer speckle pattern, however, this is close to the value expected for Fe-3 wt%Si which is 8-11%, therefore the ductility of Fe-6.5 wt%Si is likely improved when processing via AM, avoiding the ordered phases due to high cooling rates.

### 3.3. Tensile test results, epoxy reinforced

In an electrical machine, once the coils have been wound, the stator and coil assemblies are often potted with epoxy resin to ensure no movement of the coils and reduce likelihood of electrical shorting or insulation failure throughout the service life, as well as improve thermal conductivity between the parts. This potting could also be used as a way of infiltrating the cracks in this material with epoxy resin, improving the mechanical properties. Hence, this study tested 5 samples which have had the cracks filled with an epoxy resin. [Fig. 6](#) shows the stress-strain data for these samples, which show an average UTS of 25.5 MPa with a standard deviation of 5.7 MPa. There is an average of 40% improvement of the epoxy filled samples compared to the as-built samples, with a 95% increase in the minimum value to 18.8 MPa. This material would surpass the mechanical requirements needed for many electrical machine stators, including that introduced previously [19]. A two sample t-test was used to check for statistical significance between the UTS of the as-built material, and the epoxy reinforced material, resulting in a P value of 0.023, which is below the threshold of 0.05 demonstrating that the results are statistically significant.

XCT and optical microscopy were used to attempt to quantify the penetration of the epoxy into the cracks, however due to the high density of the Fe-6.5 wt%Si relative to the epoxy resin and the very small thickness of the cracks, it was not possible to clarify that the epoxy resin has infiltrated the cracks fully. The tensile test results show a significant change, therefore, it is demonstrated that the addition of the epoxy resin has caused an improvement in mechanical properties even if all of the cracks have not been fully infiltrated with epoxy. A summary of the key findings is given in [Table 1](#).

## 4. Discussion

Uniaxial tensile testing was used to gain an initial understanding into

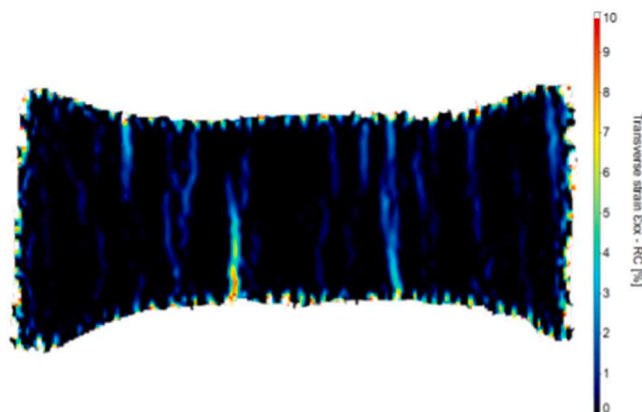


**Fig. 5.** Localised strain values prior to new crack initiation during tensile test, showing the local maximum strain is 8-10 %.

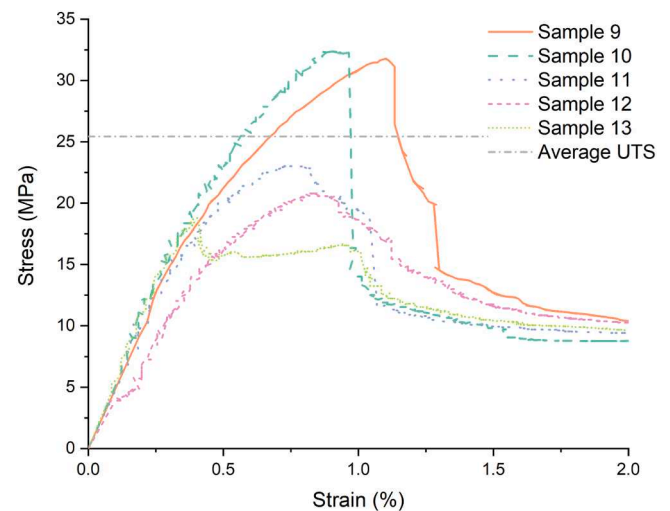


**Fig. 6.** Stress-strain data for the samples reinforced with epoxy resin, demonstrating an average UTS of 25.5 MPa.

**Table 1**

Overview of ultimate tensile properties found in this study

Sample type	Ultimate tensile stress (MPa)	Ultimate tensile stress st. dev. (MPa)	Minimum ultimate tensile stress (MPa)	Elastic modulus (GPa)	Elastic modulus st. dev. (GPa)
Solid	56.7	6.4	49.2	98.2	6.7
As-built	17.9	4.5	8.0	4.9	1.4
Epoxy filled	25.5	5.7	18.8	4.6	0.5

the behaviour of stochastically cracked soft magnetic Fe-6.5 wt%Si. Uniaxial tensile testing was chosen as it is one of the most common tests performed to understand mechanical properties, and the loading of the axial flux motor for which the loads were investigated were mostly tension. More comprehensive testing such as fatigue testing and thermal cycling will be required, however as the behaviour during uniaxial tension proved complex, further testing was outside the scope of this study.

It is important to acknowledge potential errors in the test method presented in this work. Firstly, the noise apparent in the load-displacement data is a result of a low measured load (<0.5 kN) relative to the capacity of the load cell (25 kN). A test was run for a similar period with no sample present, and the load was found to vary within +0.00050 kN and -0.00055 kN of the initial (zero) load. Similarly, the displacement varied within only +0.0018 mm and -0.0018 mm of the initial (zero) displacement. These values are small in comparison to the recorded load and variability between samples, and therefore have little impact the results of this work but create noisy data. If this work was repeated, data with less noise could be obtained by using a 1 kN or 5 kN load cell. Further to this, the clamps on the tensile test machine have a flexible coupling to prevent the introduction of non-axial forces. At these low forces, the weight of the flexible coupling causes a small non-axial force on the sample, which would normally be orders of magnitude smaller than the applied axial load. For these samples however, some visible deformation occurred during clamping and a small number of samples broke during clamping due to this. Once clamped successfully, there was often a small load already registering on the load cell. Normally this would be circumvented by using a pre-load, however the forces involved in these tests were prohibitive for applying any regular pre-load. This clamping force could introduce some non-axial force, however using DIC means that we can correlate the axial force with a transverse strain, yielding useful data.

While DIC can be a reasonable method for strain measurement, there are some limitations. For example, speckle patterns that are manually created may have a limit to the speckle size and consistency of the pattern across the sample. The speckle pattern used was created using aerosol paint giving a speckle pattern with circles approximately 0.1-0.3 mm, with occasional paint speckles up to 1 mm. Therefore, measuring maximum strain values could understate the localised maximum strain. Processing artefacts near edges and cracks may also appear artificially as areas under high strains, so maximum strain values were taken away from the edge of the sample. The size of the subset used can also influence resolution. This paper states the maximum strain to be 8-10% which would be a reasonable value for  $\alpha$ -phase non-ordered Fe-Si, but to state material properties for this material in an as-built state, further tensile tests should be carried out using fully dense material which would allow accurate measurement of the mechanical properties of the bulk material. The aims of this study were to ascertain the UTS of the material, and strain measurements were used qualitatively to gain an understanding of failure mechanism rather than absolute values. Further to this, DIC was only performed on one surface, and it may be possible that crack growth occurred or originated on another surface first or internally. Hence, there may be additional cracking that was not recorded by these images. DIC is showing data for the external surface and therefore it is not possible to infer the development of internal stresses from one DIC plot. The average UTS of the solid samples is 56.7 MPa. There is no literature available regarding the mechanical properties of additively manufactured Fe-6.5 wt%Si as most studies focus on magnetic properties. However, data from melt spun samples report an elastic modulus of 100 GPa [21], which compares well with the results in this study showing the elastic modulus is 98 GPa, though no data for ultimate tensile stress was available. A more comprehensive study into the solid samples is required to understand the low UTS of the additively manufactured samples. The parameters used were demonstrated to give density above 99.5% in  $5 \times 5 \times 5$  mm cuboidal samples, however with the larger cross-sectional area of  $25 \times 25$  mm the thermal conditions for these samples may require different process parameters to achieve high density, hence there could be some small cracking and porosity present in the solid samples which is reducing the UTS. Further to this, the as-built microstructure could yield different mechanical properties than those resulting from different manufacturing methods such as melt spinning.

The mechanical requirements for an electrical machine stator are generally low, and for the specific machine considered in this work, the required tensile stress is 7 MPa. In the as-built condition, the stochastically cracked material had an average UTS of 17.9 MPa, but with a large variability, therefore, to allow for 3 standard deviations the stress should be kept under 4.4 MPa. This would be insufficient for the application as there would be little safety factor. Reinforcing with epoxy resin improved this UTS to 25.5 MPa, and three standard deviations below would be 8.5 MPa. Therefore, even with the high variability, this material is strong enough to withstand the static loading on the stator within three standard deviations, showing promise as a soft-magnetic material that can enable 3D magnetic flux pathways, reduce eddy currents to compete with electrical steel laminations, and have sufficient mechanical properties.

It is noted that after fracture the epoxy-filled samples converge to a higher stress. Inspection of the samples reveals that this is due to a thin layer of excess epoxy on the outside of one surface of the gauge section, in the width direction, which is effectively carrying some amount of load during the final stage of the test, and therefore the test terminates with higher than zero stress as the thin area of epoxy has not broken due to its higher ductility. This does not impact the result, as the ultimate strength is still much higher in the epoxy-filled samples, and in practice, an electric motor stator prepared in this manner would also experience excess surface epoxy. It has not been shown in this study the effect the epoxy may have on the magnetic properties, though as the epoxy is replacing air, it is not expected to significantly reduce the magnetic

properties of the soft magnetic material.

Tensile testing was attempted on samples with differing gauge sections. Those with smaller gauge section ( $5 \times 2$  mm) were difficult to handle and test, however initial results suggested that the UTS was lower than samples with a larger gauge section ( $6 \times 3$  mm). With the stochastic nature of the cracking, it is possible that there is a size dependency on material properties, with very small cross-sections having decreased performance. Due to magnetic circuit requirements, the cross-sectional area is unlikely to be this small, however future work is suggested to investigate the size dependency of mechanical properties. Further, no fatigue testing has been carried out at this time. Though before usage in a machine, the thermal, magnetic, and mechanical fatigue behaviour would need to be understood. As Fe-6.5 wt%Si has very low magnetostriction (0.01 ppm [8]), thermal and mechanical fatigue are likely to be more important factors.

The cracks in this material are interconnected as shown by XCT data [18] allowing infiltrating with epoxy to be possible, which was shown to be effective in increasing the UTS. This does add a step to the manufacturing and assembly process for electrical machines, however for machines that are currently potted it is not a large change. The epoxy resin may not fully infiltrate all of the cracks; however, it has been shown to have a positive effect on the properties using the methodology in this study. Further optimisation of this filling process may allow for improved mechanical properties. Heat treatment may be required to obtain optimum magnetic properties [22], which may allow ordered phases to form in the material. This could decrease the ductility but is unlikely to have a negative effect on the UTS of the material. This heat treatment would need to be done prior to filling with epoxy, which would not interfere with the assembly process and order.

## 5. Conclusion

In the as-built condition, stochastically cracked Fe-6.5 wt%Si has inadequate mechanical properties for use in an electrical machine, owing to relatively low UTS of 17.9 MPa with a high variability ( $\sigma=4.5$  MPa). By reinforcing the material with a low-viscosity epoxy resin, mechanical properties were significantly improved, giving an average UTS of 25.5 MPa ( $\sigma=5.7$  MPa) which is statistically significant (P value 0.023). With the epoxy reinforcement this material would withstand the loading requirements of an electrical machine stator (7 MPa), giving a soft-magnetic material which can enable 3D magnetic flux pathways, with high magnetic performance and eddy current losses competitive with electrical steel laminations.

Video 1 – Video of the raw DIC data recorded showing the crack propagation.

## CRedit authorship contribution statement

**Alexander D. Goodall:** Conceptualization, Data curation, Formal analysis, Investigation, Methodology, Visualization, Writing – original draft. **Jared Uramowski:** Data curation, Formal analysis, Investigation, Methodology, Writing – review & editing. **Chad W Sinclair:** Investigation, Methodology, Supervision, Validation, Writing – review & editing. **Lova Chechik:** Visualization, Writing – review & editing. **Iain Todd:** Conceptualization, Formal analysis, Funding acquisition, Methodology, Supervision, Validation, Writing – review & editing.

## Declaration of Competing Interest

The authors declare that they have no known competing financial interests or personal relationships that could have appeared to influence the work reported in this paper.

## Data availability

Data will be made available on request.

## Acknowledgements

We wish to acknowledge the Henry Royce Institute for Advanced Materials, funded through EPSRC grants EP/R00661X/1, EP/S019367/1, EP/P02470X/1 and EP/P025285/1, for access to the AconityMINI at The University of Sheffield. We also acknowledge Sheffield Tomography Centre and University of Sheffield funding from EPSRC (EP/T006390/1) for use of the Zeiss Xradia 620 Versa X-ray microscope.

## Supplementary materials

Supplementary material associated with this article can be found, in the online version, at [doi:10.1016/j.addlet.2023.100179](https://doi.org/10.1016/j.addlet.2023.100179).

## References

- [1] M Garibaldi, I Ashcroft, M Simonelli, R. Hague, Metallurgy of high-silicon steel parts produced using selective laser melting, *Acta Mater.* 110 (2016) 207–216, <https://doi.org/10.1016/j.actamat.2016.03.037>.
- [2] B Zhang, N-E Fenineche, H Liao, C. Coddet, Microstructure and magnetic properties of Fe–Ni alloy fabricated by selective laser melting Fe/Ni mixed powders, *J. Mater. Sci. Technol.* 29 (2013) 757–760, <https://doi.org/10.1016/j.jmst.2013.05.001>.
- [3] T Riipinen, S Metsä-Kortelainen, T Lindroos, J Keränen, A Manninen, J. Pippuri-Mäkeläinen, Properties of soft magnetic Fe-Co-V alloy produced by laser powder bed fusion, *Rapid Prototyp. J.* 25 (2019) 699–707, <https://doi.org/10.1108/RPJ-06-2018-0136>.
- [4] D Goll, D Schuller, G Martinek, T Kunert, J Schurr, C Sinz, et al., Additive manufacturing of soft magnetic materials and components, *Addit. Manuf.* 27 (2019) 428–439, <https://doi.org/10.1016/j.addma.2019.02.021>.
- [5] A Plotkowski, J Pries, F List, P Nandwana, B Stump, K Carver, et al., Influence of scan pattern and geometry on the microstructure and soft-magnetic performance of additively manufactured Fe-Si, *Addit. Manuf.* 29 (2019), 100781, <https://doi.org/10.1016/j.addma.2019.100781>.
- [6] Iron - binary phase diagrams. Berlin: Düsseldorf: Springer ; Verlag Stahleisen; 1982.
- [7] JFE Steel Corporation. ELECTRICAL STEEL SHEETS n.d. <https://www.jfe-steel.co.jp/en/products/electrical/catalog/fl-e-001.pdf> (accessed July 6, 2022).
- [8] G Ouyang, X Chen, Y Liang, C Macziewski, J. Cui, Review of Fe-6.5 wt%Si high silicon steel—A promising soft magnetic material for sub-kHz application, *J. Magn. Mater.* 481 (2019) 234–250, <https://doi.org/10.1016/j.jmmm.2019.02.089>.
- [9] JNEX product data n.d.
- [10] H Seifert, M Jurisch, J Tobisch, C-G. Oertel, Mechanical properties of Fe-4.5-6wt.% Si double roller ribbons, *Mater. Sci. Eng. A* 133 (1991) 292–296, [https://doi.org/10.1016/0921-5093\(91\)90072-U](https://doi.org/10.1016/0921-5093(91)90072-U).
- [11] TF Babuska, MA Wilson, KL Johnson, SR Whetten, JF Curry, JM Rodelas, et al., Achieving high strength and ductility in traditionally brittle soft magnetic intermetallics via additive manufacturing, *Acta Mater.* 180 (2019) 149–157, <https://doi.org/10.1016/j.actamat.2019.08.044>.
- [12] AD Goodall, G Yiannakou, L Chechik, RL Mitchell, GW Jewell, I. Todd, Geometrical control of eddy currents in additively manufactured Fe-Si, *Mater. Des.* 230 (2023), 112002, <https://doi.org/10.1016/j.matdes.2023.112002>.
- [13] AD Goodall, F Nishanth, EL Severson, I. Todd, Loss performance of an additively manufactured axial flux machine stator with an eddy-current limiting structure, *Mater. Today Commun.* 35 (2023), 105978, <https://doi.org/10.1016/j.mtcomm.2023.105978>.
- [14] F Nishanth, AD Goodall, I Todd, EL. Severson, Characterization of an axial flux machine with an additively manufactured stator, *IEEE Trans. Energy Convers.* (2023) 1–13, <https://doi.org/10.1109/TEC.2023.3285539>.
- [15] A Andreiev, K-P Hoyer, D Dula, F Hengsbach, M Haase, J Gierse, et al., Soft-magnetic behavior of laser beam melted FeSi3 alloy with graded cross-section, *J. Mater. Process. Technol.* 296 (2021), 117183, <https://doi.org/10.1016/j.jmatprotec.2021.117183>.
- [16] B Koo, M-S Jang, YG Nam, S Yang, J Yu, YH Park, et al., Structurally-layered soft magnetic Fe-Si components with surface insulation prepared by shell-shaping selective laser melting, *Appl. Surf. Sci.* 553 (2021), 149510, <https://doi.org/10.1016/j.apsusc.2021.149510>.
- [17] H Tiismus, A Kallaste, A Belahcen, M Tarraste, T Vaimann, A Rassölnin, et al., AC magnetic loss reduction of SLM processed Fe-Si for additive manufacturing of electrical machines, *Energies* 14 (2021) 1241, <https://doi.org/10.3390/en14051241>.
- [18] AD Goodall, L Chechik, RL Mitchell, GW Jewell, I. Todd, Cracking of soft magnetic FeSi to reduce eddy current losses in stator cores, *Addit. Manuf.* 70 (2023), 103555, <https://doi.org/10.1016/j.addma.2023.103555>.
- [19] F Nishanth, G Bohach, MM Nahin, J Van de Ven, EL. Severson, Development of an integrated electro-hydraulic machine to electrify off-highway vehicles, *IEEE Trans. Ind. Appl.* (2022) 1–12, <https://doi.org/10.1109/TIA.2022.3189609>.
- [20] ULV #4 Ultra Low Viscosity Epoxy For Super Small Cracks n.d. <https://nextstar.ca/shop/item.aspx/ulv-4-ultra-low-viscosity-epoxy-for-super-small-cracks/12/> (accessed October 13, 2022).
- [21] G Ouyang, B Jensen, W Tang, K Dennis, C Macziewski, S Thimmaiah, et al., Effect of wheel speed on magnetic and mechanical properties of melt spun Fe-6.5 wt.% Si high silicon steel, *AIP Adv.* 8 (2018), 056111, <https://doi.org/10.1063/1.5006481>.
- [22] M Garibaldi, I Ashcroft, JN Lemke, M Simonelli, R. Hague, Effect of annealing on the microstructure and magnetic properties of soft magnetic Fe-Si produced via laser additive manufacturing, *Scr. Mater.* 142 (2018) 121–125, <https://doi.org/10.1016/j.scriptamat.2017.08.042>.